

The effect of twist-bend coupling on the torsional properties of double-stranded DNA

S. K. Nomidis,¹ W. Vanderlinden,^{2,3} J. Lipfert,³ and E. Carlon¹

¹*KU Leuven, Institute for Theoretical Physics, Celestijnenlaan 200D, 3001 Leuven, Belgium*

²*KU Leuven, Department of Chemistry, 3001 Leuven, Belgium*

³*Department of Physics, Nanosystems Initiative Munich, and Center for NanoScience, Ludwig Maximilians University Munich, 80799 Munich, Germany*

(Dated: December 3, 2024)

Single-molecule magnetic tweezers experiments performed in the past few years report a clear deviation of the effective torsional stiffness of DNA from the predictions of the twistable worm-like chain model. Here we show that this discrepancy can be resolved if a coupling term between bending and twisting is introduced. Although the existence of such an interaction was predicted more than two decades ago (Marko and Siggia, *Macromol.* **27**, 981 (1994)), its effect on the static and dynamical properties of DNA has been largely unexplored. Our analysis yields a twist-bend coupling constant of $G = 50 \pm 10$ nm. We show that the introduction of twist-bend coupling requires a re-tuning of the other elastic parameters of DNA, in particular for the intrinsic bending stiffness.

PACS numbers: 87.17.Aa, 87.16.Yc, 82.40.Bj, 87.18.Vf

The mechanical properties of DNA are of great importance for both its structure and its functioning within the cell. In vivo, DNA is able to bend and twist and these mechanical deformations influence its interaction with other molecules (see e.g. [1]). In order to understand the static and dynamical properties of DNA and its plethora of interactions, it is important to have an accurate physical model with the correct parametrization.

The standard model for double-stranded DNA (dsDNA) at length scales larger than one helical turn (about 10.5 base pairs) is the twistable worm-like chain (TWLC) model, which treats the molecule as a continuous and isotropic elastic rod [2]. The TWLC model features four elastic parameters, namely the bending stiffness A , the torsional stiffness C , the stretch modulus S and the twist-stretch coupling constant D . For stretching forces below 10 pN (the range of values considered here) DNA is practically inextensible, therefore the stretch and twist-stretch deformations can be neglected. The TWLC model describes very well many of the dsDNA properties and fits of the model to experimental data have enabled precise determination of the elastic parameters. Measurements of the stretching response under an applied force yield $A \approx 50$ nm [3, 4], while studies of the torsional response under an applied twist give $C \approx 110$ nm [5, 6]. Note that the value of C has undergone several refinements in the past with the initial estimations being in the range 35 – 90 nm [7].

Despite its successes, there are experimental observations that the TWLC model fails to account for quantitatively. Notably, a series of single-molecule experiments has shown that the resistance of dsDNA against a twist deformation decreases with the applied force [5, 6, 8, 9]. While the TWLC model predicts the right trend qualitatively [10], there are significant deviations from magnetic tweezers (MT) data [6]. The aim of this letter is to discuss the origin of these deviations and propose a solution

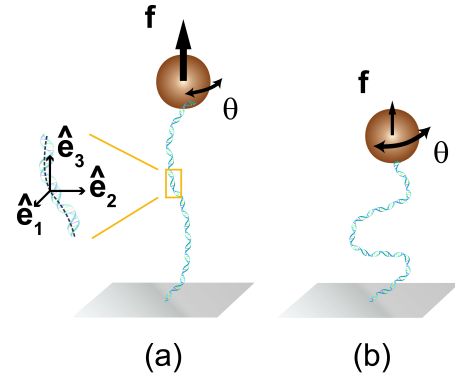


FIG. 1. Schematic representation of a typical MT experiment, in which a dsDNA molecule is stretched by a force \mathbf{f} and twisted by an angle θ . The effective torsional stiffness, which expresses its resistance to the twist, is higher at stronger forces (a) and lower at weaker ones (b), where twist is partially “absorbed” by bending fluctuations.

to this issue.

Fig. 1 illustrates the setup of a typical MT experiment, in which the two ends of the molecule are attached to a solid substrate and a paramagnetic bead. A set of magnets placed above the bead exert a linear force f and/or torque to it. At forces above $f \approx 5$ pN (Fig. 1a) the DNA molecule is elongated to approximately 90% of its full length and the response to the twist is basically governed by the intrinsic torsional stiffness constant C . At lower forces (Fig. 1b), however, the twist imposed on the bead can be significantly “absorbed” by bending fluctuations [10], thus leading to a decrease in the resistance to a twist deformation. One then measures an *effective* torsional stiffness $C_{\text{eff}}(f)$, which is an increasing function of the applied force f .

This force dependence of the effective torsional stiffness was investigated in the framework of the TWLC

model by Moroz and Nelson [10, 11], who analytically derived a high force expansion for $C_{\text{eff}}(f)$. While that expansion predicts the right trend qualitatively, the experimental data fall below the analytical predictions at forces weaker than 2 pN [6, 9], still well within the range of applicability of the model. Here we show that these deviations can be explained within the framework of an extended TWLC model, which was already introduced by Marko and Siggia more than two decades ago [12] (from now on we will refer to it as the MS model). This is a generalization of the standard TWLC model, that contains two additional features: an anisotropic bending term, which makes the molecule easier to bend along a particular direction, and a twist-bend coupling one. The effect of bending anisotropy on the mechanical behavior of dsDNA has been studied by several authors in the past [13–15]. The twist-bend coupling, however, remains to date largely unexplored. A notable exception is Ref. [16], in which the experimental structure of dsDNA wrapped around a histone was analyzed, concluding that the elastic correlations can be explained by a non-zero twist-bend coupling. Here we show that, by introducing twist-bend coupling, one can quantitatively reproduce the measured dependence of C_{eff} on the applied force.

Following the same approach as in [12], we model DNA as an inextensible, elastic rod of length L . An orthonormal set of vectors $\{\hat{\mathbf{e}}_1, \hat{\mathbf{e}}_2, \hat{\mathbf{e}}_3\}$ is associated with every point along the chain (see Fig. 1). Here $\hat{\mathbf{e}}_3$ is the tangent to the curve and $\hat{\mathbf{e}}_1$ points from the center of the helix towards its minor groove. The third vector is obtained from the relation $\hat{\mathbf{e}}_2 = \hat{\mathbf{e}}_3 \times \hat{\mathbf{e}}_1$. In a relaxed dsDNA molecule, the helical axis is completely straight, corresponding to $\hat{\mathbf{e}}_3(s)$ being constant along the chain, where $0 \leq s \leq L$ is the arc length. The double helix makes a full turn every $l = 2\pi/\omega_0 \approx 3.4$ nm, which means that $\hat{\mathbf{e}}_1(s)$ and $\hat{\mathbf{e}}_2(s)$ are rotated by an angle of $\omega_0 s$ with respect to $\hat{\mathbf{e}}_1(0)$ and $\hat{\mathbf{e}}_2(0)$. Any deformation from this ideal state can be described by the relation [12]

$$\frac{d\hat{\mathbf{e}}_i}{ds} = (\omega_0 \hat{\mathbf{e}}_3 + \boldsymbol{\Omega}) \times \hat{\mathbf{e}}_i, \quad (1)$$

where $\Omega_i(s)ds$ is defined as the deformation angle around $\hat{\mathbf{e}}_i(s)$, i.e. the angle by which the set $\{\hat{\mathbf{e}}_1, \hat{\mathbf{e}}_2, \hat{\mathbf{e}}_3\}$ is rotated when going from s to $s + ds$. As discussed in [12], the symmetry of dsDNA implies an invariance of its mechanical energy with respect to the operation $\Omega_1 \rightarrow -\Omega_1$. For small deformations one may expand the energy of the system around the minimum at $\boldsymbol{\Omega} = \mathbf{0}$ and show that, to lowest orders, the energy takes the form [12]

$$\beta E_{\text{MS}} = \frac{1}{2} \int_0^L ds (A_1 \Omega_1^2 + A_2 \Omega_2^2 + C \Omega_3^2 + 2G \Omega_2 \Omega_3), \quad (2)$$

where $\beta \equiv 1/k_B T$ is the inverse temperature. The parameters A_1 , A_2 , C and G have the dimension of length and quantify the energetic cost of different deformations.

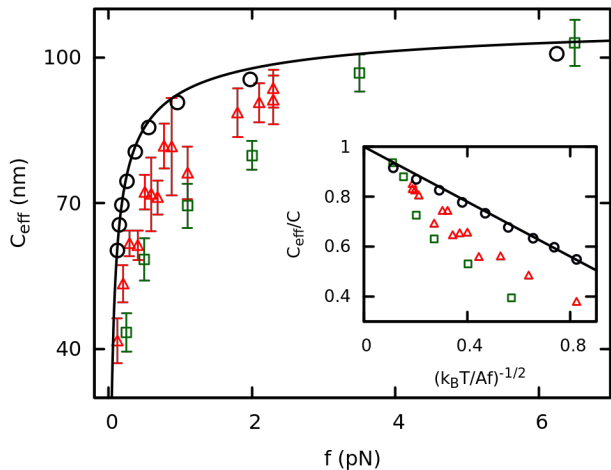


FIG. 2. Main frame: Effective torsional stiffness C_{eff} as a function of the stretching force f . Two independent experiments from magnetic torque tweezers (green squares) [6] and freely orbiting magnetic tweezers (red triangles) [9] show a clear deviation from the TWLC prediction (Eq. (4), shown as solid line) and computer simulations of the standard TWLC model (empty circles, with error-bars smaller than the symbol sizes). Inset: the same data are plotted in rescaled, dimensionless units, in which Eq. (4) becomes a straight line.

A_1 and A_2 are associated with bending along planes perpendicular to $\hat{\mathbf{e}}_1$ and $\hat{\mathbf{e}}_2$, respectively. C is the *intrinsic* torsional stiffness and quantifies the energetic cost of a twist deformation, i.e. a rotation around $\hat{\mathbf{e}}_3$. G is the coupling between twisting (Ω_3) and bending (Ω_2). Cylindrical symmetry would imply $A_1 = A_2 = A$ (isotropic bending) and $G = 0$ (no twist-bend coupling) [12], so that the Eq. (2) reduces to that of the standard inextensible TWLC model

$$\begin{aligned} \beta E_{\text{TWLC}} &= \frac{1}{2} \int_0^L ds [A (\Omega_1^2 + \Omega_2^2) + C \Omega_3^2] \\ &= \frac{1}{2} \int_0^L ds \left[A \left(\frac{d\hat{\mathbf{e}}_3}{ds} \right)^2 + C \Omega_3^2 \right], \quad (3) \end{aligned}$$

where we have also used Eq. (1) to rewrite the bending term.

Computer simulations of the TWLC and the MS models were performed using a coarse-grained bead-and-spring polymer similar to that discussed in [17]. Each bead behaves as a rigid, spherical body, consisting of a core atom and three small patches at fixed distance from the core defining the local frame $\{\hat{\mathbf{e}}_1, \hat{\mathbf{e}}_2, \hat{\mathbf{e}}_3\}$. The two ends of the polymer were attached to an impenetrable surface and a large bead, similarly to a typical MT experiment setup. The equilibrium conformations of the molecule were sampled by means of a Langevin dynamics integrator (implicit solvent), using the Large-scale Atomic/Molecular Massively Parallel Simulator (LAMMPS) [18]. The effective torsional stiff-

ness was calculated from the relation $C_{\text{eff}} = L/\sigma_\theta^2$, where L is the total length of the polymer and σ_θ^2 is the variance of the twist angle.

Moroz and Nelson [10] derived the following relation for the effective torsional stiffness of the TWLC

$$C_{\text{eff}} = C \left(1 - \frac{C}{4A} \sqrt{\frac{k_B T}{Af}} + \dots \right), \quad (4)$$

which is an asymptotic expansion at large forces. In Fig. 2 we plot this expression using the accepted values $A = 50$ nm and $C = 110$ nm [19], together with the data of two independent MT experimental studies [6, 9]. Although both theory and experiments are in qualitative agreement, there is a significant deviation between the two at weak forces. Simulation data of the TWLC model (empty circles in Fig. 2) are in excellent agreement with Eq. (4). This confirms that higher-order corrections to this equation can be safely neglected [10] for the range of forces considered in MT experiments.

We now turn to the analysis of the MS model, which contains four parameters (Eq. (2)). These should be tuned so that the known physical properties of dsDNA are reproduced. For this purpose we have derived analytical expressions for the bending and twisting persistence lengths of the MS model for a free, relaxed molecule (the derivation can be found in the supplemental material). The bending persistence length is given by

$$l_b = A \frac{1 - \frac{\varepsilon^2}{A^2} - \frac{G^2}{AC} \left(1 + \frac{\varepsilon}{A}\right)}{1 - \frac{G^2}{2AC}}, \quad (5)$$

where we have introduced the mean bending stiffness $A \equiv (A_1 + A_2)/2$ and the bending anisotropy $\varepsilon \equiv (A_1 - A_2)/2$. The twist persistence length is given by the relation

$$l_t = C \frac{1 - \frac{\varepsilon}{A} - \frac{G^2}{AC}}{1 - \frac{\varepsilon}{A}}. \quad (6)$$

By setting $\varepsilon = G = 0$ in these expressions, we recover the limiting values $l_b = A$ and $l_t = C$, i.e. in the TWLC model the stiffness parameters A and C are also the persistence lengths [2]. This is not the case in the MS model, however, for which Eqs. (5) and (6) imply that $l_b < A$ and $l_t < C$. These equations also reproduce some other known limiting cases. For instance, upon setting $G = 0$ one finds $l_b^{-1} = (A_1^{-1} + A_2^{-1})/2$, which has been discussed in [20, 21], whereas for $\varepsilon = 0$ and small G , one gets $l_b \approx A - G^2/2C$, a perturbative result reported in [12].

In the simulations we set the intrinsic torsional stiffness at $C = 110$ nm, i.e. the plateau value of C_{eff} at high forces (see Fig. 2). In this regime bending fluctuations become negligible ($\Omega_1, \Omega_2 \approx 0$) and the torsional response is governed by C (see Eq. (2)). Following Ref. [13], we

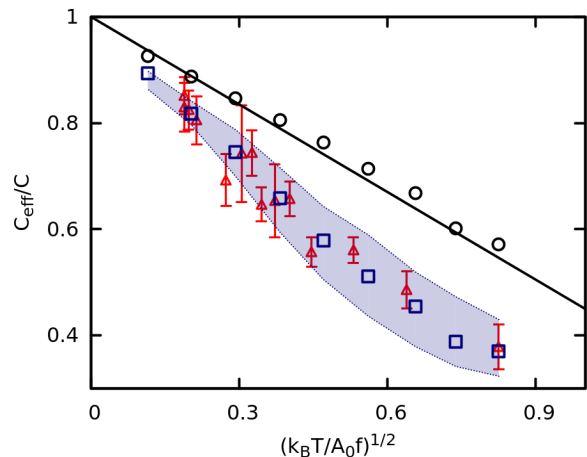


FIG. 3. Effective torsional stiffness as a function of the applied force in rescaled, dimensionless units (with $A_0 = 50$ nm). Simulations of the MS model (blue squares) are in excellent agreement with the experimental data (red triangles, taken from [9]). We thus conclude that a non-zero twist-bend coupling of $G = 50 \pm 10$ nm (in dotted, blue lines, from top to bottom, are simulations for $G = 40$ nm and $G = 60$ nm.) can explain reported deviation from the theory (solid line). Note that a non-zero bending anisotropy alone ($G = 0$ with black circles) cannot account for this discrepancy. The errors in the simulation data are smaller than the size of the points.

choose a representative value $\varepsilon = 20$ nm for the bending anisotropy. Next we select the values of G and A according to Eq. (5), so as to make sure that $l_b = 50$ nm, which is the measured persistence length of dsDNA [2]. There is therefore only one parameter, namely G , which can be freely adjusted.

In Fig. 3 we plot simulation data of the effective torsional stiffness versus the square root of the inverse force in rescaled, dimensionless units. As we compute C_{eff} from the fluctuations of the twist angle, we compare our simulations to freely orbiting MT experiments [9], which are based on the same principle. A good agreement with the experimental data (red triangles in Fig. 3) is found for $G = 50$ nm (blue squares), which requires $A \approx 76.5$ nm in order to ensure that $l_b = 50$ nm (see Eq.(5)). The shaded area corresponds to simulations with G within the range 40 – 60 nm, which covers well the experimental uncertainties. In order to test the effect of pure anisotropic bending, a set of simulations was performed with $G = 0$, $\varepsilon = 20$ nm and $A \approx 57$ nm, again keeping $l_b = 50$ nm. The result is shown with black circles in Fig. 3 and barely deviates from Eq. (4). This shows that the bending anisotropy alone has a rather weak effect on C_{eff} , as it could have been guessed from Eq. (6), i.e. from the weak dependence of twisting persistence length on ε , when $G = 0$. We thus conclude that, within the framework of the MS model, twist-bend coupling is necessary in order to reproduce the experimental C_{eff} data.

Note that the previous estimate $G = 25$ nm of the twist-bend coupling constant [16] is substantially lower than the value found in our simulations. However, in that study the elastic parameters had not been tuned according to Eqs. (5) and (6), hence the resulting persistence lengths of dsDNA were smaller than the experimentally established ones.

An alternative explanation for the deviations between the measured effective torsional stiffness and Eq. (4) was proposed by Schurr [22], who invoked a cooperative transition between two conformations of the DNA double helix, which have a different torsional stiffness and rise per base pair. While this model, too, describes the experimental data [22], there is at the moment no independent evidence for the proposed conformational transition. In contrast, the twist-bend coupling naturally arises from the symmetry of the dsDNA molecule [12] and has been invoked in past, in order to explain some structural correlation of DNA wrapped around histones [16].

Another interesting property of the MS model is that the twisting persistence length l_t and the intrinsic torsional stiffness C are, in general, different ($l_t < C$), in contrast to the TWLC model for which it is always $l_t = C$. This may explain the low value of C obtained from several experimental techniques, such as the fluorescence polarization anisotropy (FPA), which probe the twisting persistence length l_t rather than the elastic constant C . Eq. (6), together with the parameters $C = 110$ nm, $G = 50$ nm, $\varepsilon = 20$ and $A \approx 76.5$ nm we used here, yield $l_t \approx 65.7$ nm, which is close to the range of measured values from FPA studies (e.g. Ref. [23] reports 50 nm).

Finally, we discuss the dependence of the elongation z of DNA, as a function of the applied twist. If the twist angle θ exceeds a critical value, z starts decreasing sharply, which is a signature of the transition to a supercoiled state [1]. For smaller values of θ , i.e. when the DNA is in the normal, elongated state, z decreases weakly with θ . The origin of this effect is similar to that of Eq. (4), i.e. the molecule contracts in order to reduce the torsional stress, by increasing the bending fluctuations. Moroz and Nelson [10] and Bouchiat and Mezard [24] analyzed this dependence of z on the twist angle θ , as a function of applied force, using the TWLC model, which turned out to fit well the experimental data.

In Fig. 4 we show this dependence, using data from MT experiments and simulations of both the TWLC and MS models for three different values of the applied force. The black arrows denote our estimate of the onset of the supercoiling transition. Simulations show that in the normal (i.e. non-supercoiled) state both models fit equally well the experiments. Significant differences are, however, observed in the supercoiled state, i.e. for larger applied twist, with the MS model starting deviating from the experimental data. This region is beyond the limit of validity of the expansion (2) in small Ω 's and higher-order

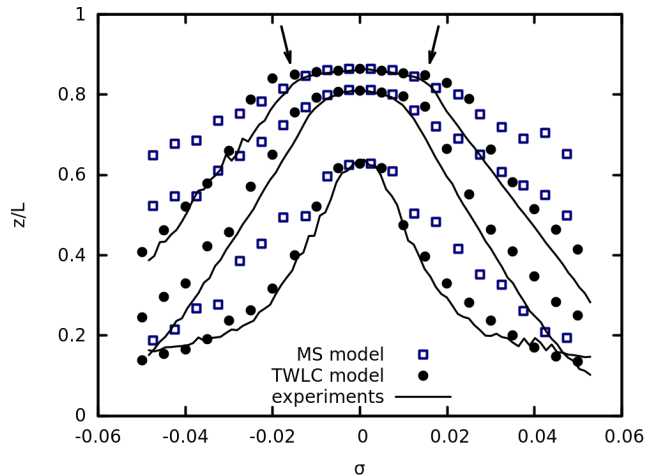


FIG. 4. Relative extension z/L of a dsDNA molecule versus the supercoiling density $\sigma \equiv \theta/\omega_0 L$, for three different forces ($f = 1$ pN, $f = 0.5$ pN and $f = 0.1$ pN, from top to bottom). We have defined z the elongation of the molecule, L the contour length and θ the twist angle. The experimental data from MT (black lines) agree very well with computer simulations of both the TWLC model (black points) and the MS one (blue squares) for small values of σ . Beyond a critical value (black arrows in the top curve) DNA supercoils, leading to a sharp decrease in the extension. In that region the MS model agrees less well, probably because the expansion (2) ceases to be valid at strong, local deformations.

interactions possibly start playing an important role. In both simulations of Fig. 4, a simple, soft, repulsive potential between the beads was used. It is, thus, possible that more complex interactions have to be taken into account, in order to properly reproduce the supercoiling data.

Summarizing, we have proposed a solution to the discrepancy [6] between the experimentally determined effective torsional stiffness and the predictions of the TWLC model. Our simulations show that the experimental data are well-fitted by an extended model, proposed long ago by Marko and Siggia [12], and have highlighted the crucial role of the twist-bend coupling. The introduction of this new coupling constant requires a re-tuning of the existing elastic parameters of DNA, in order to keep the experimentally established values of the persistence lengths unchanged.

-
- [1] J. F. Marko, *Physica A* **418**, 126 (2015).
 - [2] P. Nelson, M. Radosavljevic, and S. Bromberg, *Biological physics: energy, information, life* (W.H. Freeman and Co., New York, 2002).
 - [3] C. Bustamante, J. Marko, E. Siggia, and B. Smith, *Science* **265** (1994).
 - [4] C. G. Baumann, S. B. Smith, V. A. Bloomfield, and C. Bustamante, *Proc. Natl. Acad. Sci. USA* **94**, 6185

- (1997).
- [5] Z. Bryant, M. D. Stone, J. Gore, S. B. Smith, N. R. Cozzarelli, and C. Bustamante, *Nature* **424**, 338 (2003).
 - [6] J. Lipfert, J. W. Kerssemakers, T. Jager, and N. H. Dekker, *Nat. Methods* **7**, 977 (2010).
 - [7] A. V. Vologodskii, S. D. Levene, K. V. Klenin, M. Frank-Kamenetskii, and N. R. Cozzarelli, *J. Mol. Biol.* **227**, 1224 (1992).
 - [8] F. Mosconi, J. F. Allemand, D. Bensimon, and V. Croquette, *Phys. Rev. Lett.* **102**, 078301 (2009).
 - [9] J. Lipfert, M. Wiggin, J. W. Kerssemakers, F. Pedaci, and N. H. Dekker, *Nat. Commun.* **2**, 439 (2011).
 - [10] J. D. Moroz and P. Nelson, *Proc. Natl. Acad. Sci. U.S.A.* **94**, 14418 (1997).
 - [11] J. D. Moroz and P. Nelson, *Macromolecules* **31**, 6333 (1998).
 - [12] J. Marko and E. Siggia, *Macromolecules* **27**, 981 (1994).
 - [13] D. Norouzi, F. Mohammad-Rafiee, and R. Golestanian, *Phys. Rev. Lett.* **101**, 168103 (2008).
 - [14] B. Eslami-Mossallam and M. Ejtehadi, *Phys. Rev. E* **80**, 011919 (2009).
 - [15] H. Salari, B. Eslami-Mossallam, S. Naderi, and M. Ejtehadi, *J. Chem. Phys.* **143**, 104904 (2015).
 - [16] F. Mohammad-Rafiee and R. Golestanian, *Phys. Rev. Lett.* **94**, 238102 (2005).
 - [17] C. Brackley, A. Morozov, and D. Marenduzzo, *J. Chem. Phys.* **140**, 135103 (2014).
 - [18] S. Plimpton, *J. Comp. Phys.* **117**, 1 (1995).
 - [19] J. Lipfert, G. M. Skinner, J. M. Keegstra, T. Hensgens, T. Jager, D. Dulin, M. Köber, Z. Yu, S. P. Donkers, F.-C. Chou, *et al.*, *Proc. Natl. Acad. Sci. USA* **111**, 15408 (2014).
 - [20] F. Lankaš, J. Šponer, P. Hobza, and J. Langowski, *J. Mol. Biol.* **299**, 695 (2000).
 - [21] B. Eslami-Mossallam and M. Ejtehadi, *J. Chem. Phys.* **128**, 125106 (2008).
 - [22] J. M. Schurr, *J. Phys. Chem. B* **119**, 6389 (2015).
 - [23] J. H. Shibata, B. S. Fujimoto, and J. M. Schurr, *Biopolymers* **24**, 1909 (1985).
 - [24] C. Bouchiat and M. Mézard, *Phys. Rev. Lett.* **80**, 1556 (1997).

SUPPLEMENTAL MATERIAL

Analysis of the MS model

In this section we present in detail an exact calculation of the bending and torsional persistence lengths (l_b and l_t , respectively) for the MS model.

Defining $A_1 = A + \varepsilon$ and $A_2 = A - \varepsilon$, we write the energy of the model as follows

$$\frac{E_{\text{MS}}}{k_B T} = \frac{1}{2} \int_0^L ds (A_1 \Omega_1^2 + A_2 \Omega_2^2 + C \Omega_3^2 + 2G \Omega_2 \Omega_3) = \frac{E_{\text{TWLC}}}{k_B T} + \int_0^L ds \left[\frac{\varepsilon}{2} (\Omega_1^2 - \Omega_2^2) + G \Omega_2 \Omega_3 \right], \quad (7)$$

where E_{TWLC} indicates the energy of the standard TWLC model and the two additional terms are the contributions from the bending anisotropy ($\varepsilon \neq 0$) and the twist-bend coupling ($G \neq 0$). Using this expression as a starting point, we are going to derive Eqs. (40) and (42), which describe the ε and G dependence of the persistence lengths.

To start we need to express $\{\Omega_i\}$ as functions of the vectors $\{\hat{\mathbf{e}}_i\}$ and their derivatives. For this purpose we use the relations

$$\frac{d\hat{\mathbf{e}}_1}{ds} = (\omega_0 + \Omega_3) \hat{\mathbf{e}}_2 - \Omega_2 \hat{\mathbf{e}}_3 \quad (8)$$

$$\frac{d\hat{\mathbf{e}}_2}{ds} = \Omega_1 \hat{\mathbf{e}}_3 - (\omega_0 + \Omega_3) \hat{\mathbf{e}}_1 \quad (9)$$

$$\frac{d\hat{\mathbf{e}}_3}{ds} = \Omega_2 \hat{\mathbf{e}}_1 - \Omega_1 \hat{\mathbf{e}}_2. \quad (10)$$

Next we discretize the model introducing a discretization length a and using the following approximations

$$\frac{d\hat{\mathbf{e}}_i(s)}{ds} \simeq \frac{\hat{\mathbf{e}}_i(s+a) - \hat{\mathbf{e}}_i(s)}{a} \quad (11)$$

$$\hat{\mathbf{e}}_i(s) \simeq \frac{\hat{\mathbf{e}}_i(s+a) + \hat{\mathbf{e}}_i(s)}{2}. \quad (12)$$

In order to parametrize the rotation of the frame $\{\hat{\mathbf{e}}_1(s), \hat{\mathbf{e}}_2(s), \hat{\mathbf{e}}_3(s)\}$ into $\{\hat{\mathbf{e}}_1(s+a), \hat{\mathbf{e}}_2(s+a), \hat{\mathbf{e}}_3(s+a)\}$, we introduce three Euler angles $\alpha(s)$, $\beta(s)$ and $\gamma(s)$. These angles correspond to a sequence of three elementary rotations: one about $\hat{\mathbf{e}}_3$, followed by one about $\hat{\mathbf{e}}_1$ and finally a rotation about $\hat{\mathbf{e}}_3$, respectively:

$$\hat{\mathbf{e}}_i(s+a) = \sum_{j=1}^3 R_{ij}(\alpha, \beta, \gamma) \hat{\mathbf{e}}_j(s), \quad (13)$$

where R is the product of three rotation matrices

$$R = E_3(\gamma) E_1(\beta) E_3(\alpha) \quad (14)$$

with

$$E_1(\phi) = \begin{pmatrix} 1 & 0 & 0 \\ 0 & \cos \phi & \sin \phi \\ 0 & -\sin \phi & \cos \phi \end{pmatrix} \quad (15)$$

$$E_3(\phi) = \begin{pmatrix} \cos \phi & \sin \phi & 0 \\ -\sin \phi & \cos \phi & 0 \\ 0 & 0 & 1 \end{pmatrix}. \quad (16)$$

From the above definitions we get

$$R = \begin{pmatrix} \cos \alpha \cos \gamma - \sin \alpha \cos \beta \sin \gamma & \sin \alpha \cos \gamma + \cos \alpha \cos \beta \sin \gamma & \sin \beta \sin \gamma \\ -\cos \alpha \sin \gamma - \sin \alpha \cos \beta \cos \gamma & -\sin \alpha \sin \gamma + \cos \alpha \cos \beta \cos \gamma & \sin \beta \cos \gamma \\ \sin \alpha \sin \beta & -\cos \alpha \sin \beta & \cos \beta \end{pmatrix}. \quad (17)$$

Combining the above relations yields

$$\begin{aligned}\Omega_1^2 &= \hat{\mathbf{e}}_1 \cdot \frac{d\hat{\mathbf{e}}_2}{ds} \times \frac{d\hat{\mathbf{e}}_3}{ds} = \frac{\hat{\mathbf{e}}_1(s+a) \cdot \hat{\mathbf{e}}_1(s)}{2} \cdot \frac{\hat{\mathbf{e}}_2(s+a) - \hat{\mathbf{e}}_2(s)}{a} \times \frac{\hat{\mathbf{e}}_3(s+a) - \hat{\mathbf{e}}_3(s)}{a} \\ &= \frac{1 + \hat{\mathbf{e}}_1(s+a) \cdot \hat{\mathbf{e}}_1(s) - \hat{\mathbf{e}}_2(s+a) \cdot \hat{\mathbf{e}}_2(s) - \hat{\mathbf{e}}_3(s+a) \cdot \hat{\mathbf{e}}_3(s)}{a^2} = \frac{1 + R_{11} - R_{22} - R_{33}}{a^2} \\ &= \frac{(1 - \cos \beta) [1 + \cos(\alpha - \gamma)]}{a^2}\end{aligned}\quad (18)$$

$$\Omega_2^2 = \hat{\mathbf{e}}_2 \cdot \frac{d\hat{\mathbf{e}}_3}{ds} \times \frac{d\hat{\mathbf{e}}_1}{ds} = \frac{(1 - \cos \beta) [1 - \cos(\alpha - \gamma)]}{a^2}\quad (19)$$

and hence

$$\Omega_1^2 + \Omega_2^2 = \frac{2}{a^2} (1 - \cos \beta)\quad (20)$$

$$\Omega_1^2 - \Omega_2^2 = \frac{2}{a^2} (1 - \cos \beta) \cos(\alpha - \gamma).\quad (21)$$

The other two terms appearing in Eq. (7) are

$$\Omega_3^2 = \hat{\mathbf{e}}_3 \cdot \left(\frac{d\hat{\mathbf{e}}_1}{ds} - \omega_0 \hat{\mathbf{e}}_2 \right) \times \left(\frac{d\hat{\mathbf{e}}_2}{ds} + \omega_0 \hat{\mathbf{e}}_1 \right) = \frac{(1 + \cos \beta) [1 - \cos(\alpha + \gamma) - a\omega_0 \sin(\alpha + \gamma)] + a^2 \omega_0^2}{a^2}\quad (22)$$

$$\Omega_2 \Omega_3 = -\frac{d\hat{\mathbf{e}}_3}{ds} \cdot \left(\frac{d\hat{\mathbf{e}}_2}{ds} + \omega_0 \hat{\mathbf{e}}_1 \right) = \frac{\sin \beta [2(\cos \gamma - \cos \alpha) + a\omega_0 (\sin \alpha - \sin \gamma)]}{2a^2}.\quad (23)$$

In the continuum limit $a \rightarrow 0$, the Euler angles become infinitesimally small, i.e. $\alpha, \beta, \gamma \rightarrow 0$. This allows us to approximate

$$1 + \cos \beta \simeq 2\quad (24)$$

$$\cos \alpha + \frac{a\omega_0}{2} \sin \alpha \simeq \cos(\alpha - \phi_0)\quad (25)$$

$$\cos \gamma + \frac{a\omega_0}{2} \sin \gamma \simeq \cos(\gamma - \phi_0)\quad (26)$$

$$\cos(\alpha + \gamma) + a\omega_0 \sin(\alpha + \gamma) \simeq \cos(\alpha + \gamma - 2\phi_0),\quad (27)$$

where we have defined

$$\phi_0 \equiv \frac{a\omega_0}{2} \simeq \sin\left(\frac{a\omega_0}{2}\right)\quad (28)$$

and made use of $\cos \phi_0 \simeq 1$. With the above approximations we get

$$\Omega_3^2 = \frac{2}{a^2} [1 - \cos(\alpha + \gamma - 2\phi_0)] + \omega_0^2\quad (29)$$

$$\Omega_2 \Omega_3 = -\frac{1}{a^2} \sin \beta [\cos(\alpha - \phi_0) - \cos(\gamma - \phi_0)].\quad (30)$$

Substituting Eqs. (20), (21), (29) and (30) into (7) and transforming the integral into a sum over segments of length a ($\int_0^L ds \dots \simeq a \sum_i \dots$) yields

$$\begin{aligned}\frac{E_{\text{MS}}}{k_B T} &= -\frac{1}{a} \sum_i \{A \cos \beta_i + C \cos(\alpha_i + \gamma_i - 2\phi_0) - \varepsilon (1 - \cos \beta_i) \cos(\alpha_i - \gamma_i) \\ &\quad + G \sin \beta_i [\cos(\alpha_i - \phi_0) - \cos(\gamma_i - \phi_0)]\},\end{aligned}\quad (31)$$

where we have omitted any constant terms. One can simplify this expression by introducing the angles $\psi_i \equiv \alpha_i + \gamma_i - 2\phi_0$ and $\chi_i \equiv \alpha_i - \gamma_i$, so as to obtain

$$\frac{E_{\text{eTWLC}}}{k_B T} = -\frac{1}{a} \sum_i \left[A \cos \beta_i + C \cos \psi_i - \varepsilon (1 - \cos \beta_i) \cos \chi_i - 2G \sin \frac{\chi_i}{2} \sin \frac{\psi_i}{2} \sin \beta_i \right].\quad (32)$$

where β_i and ψ_i are bending and twist angles, respectively.

The total partition function can be written as

$$Z = \prod_i \left(\int d\beta_i \sin \beta_i d\psi_i d\chi_i \right) e^{-E_e \text{TWLC} / k_B T}, \quad (33)$$

where $\beta_i \in [0, \pi]$ and $\psi_i, \chi_i \in [-\pi, \pi]$. As the total energy is the sum of independent contributions, it is sufficient to consider the partition function of a single segment

$$Z_{\text{segm}} = \int_0^\pi d\beta \sin \beta \int_{-\pi}^\pi d\psi \int_{-\pi}^\pi d\chi \exp \left\{ \frac{1}{a} \left[A \cos \beta + C \cos \psi - \varepsilon (1 - \cos \beta) \cos \chi - 2G \sin \frac{\chi}{2} \sin \frac{\psi}{2} \sin \beta \right] \right\}. \quad (34)$$

We require that the quadratic form (7) is positive [1] so that the minimum of the energy corresponds to a straight ($\beta = 0$) and untwisted ($\psi = 0$) conformation. The minimum does not depend on the value of χ . In the limit $a \rightarrow 0$ we can expand the trigonometric functions in Eq. (34) around $\beta = \psi = 0$ and extend the integration domains of these two variables to ∞

$$\begin{aligned} Z_{\text{segm}} &\simeq e^{(A+C)/a} \int_{-\pi}^\pi d\chi \int_0^\infty d\beta \beta \exp \left[-\frac{\beta^2}{2a} (A + \varepsilon \cos \chi) \right] \int_{-\infty}^\infty d\psi \exp \left[-\frac{C}{2a} \left(\psi^2 + \frac{2G}{C} \sin \frac{\chi}{2} \beta \psi \right) \right] \\ &= \dots \frac{e^{(A+C)/a}}{\sqrt{C}} \int_{-\pi}^\pi d\chi \int_0^\infty d\beta \beta^2 \exp \left[-\frac{\beta^2}{2a} \left(A + \varepsilon \cos \chi - \frac{G^2}{C} \sin^2 \frac{\chi}{2} \right) \right] \\ &= \dots \frac{e^{(A+C)/a}}{\sqrt{C}} \int_{-\pi}^\pi d\chi \frac{d\chi}{A - G^2/2C + (\varepsilon + G^2/2C) \cos \chi} \\ &= \dots \frac{e^{(A+C)/a}}{\sqrt{C}} \left[\left(A - \frac{G^2}{2C} \right)^2 - \left(\varepsilon + \frac{G^2}{2C} \right)^2 \right]^{-1/2} = \dots \frac{e^{(A+C)/a}}{\sqrt{C}} \left[(A + \varepsilon) \left(A - \varepsilon - \frac{G^2}{C} \right) \right]^{-1/2}, \quad (35) \end{aligned}$$

where the dots (...) denote numerical prefactors which can be ignored, since they do not contribute to thermal averages.

We are interested in the following averages

$$\langle \cos \beta \rangle = a \frac{\partial}{\partial A} \ln Z_{\text{segm}} = 1 - \frac{a}{A} \frac{1 - \frac{G^2}{2AC}}{1 - \frac{\varepsilon^2}{A^2} - \frac{G^2}{AC} \left(1 + \frac{\varepsilon}{A} \right)} \quad (36)$$

and

$$\langle \cos(\alpha + \gamma - 2\phi_0) \rangle = a \frac{\partial}{\partial C} \ln Z_{\text{segm}} = 1 - \frac{a}{2C} \frac{1 - \frac{\varepsilon}{A}}{1 - \frac{\varepsilon}{A} - \frac{G^2}{AC}}, \quad (37)$$

since from these one can compute correlation functions. For instance, bending correlations are given by

$$\langle \hat{\mathbf{e}}_3(0) \cdot \hat{\mathbf{e}}_3(na) \rangle = \langle \cos \beta_1 \cos \beta_2 \dots \cos \beta_n \rangle = \langle \cos \beta \rangle^n \equiv e^{-na/l_b}, \quad (38)$$

where l_b is the bending persistence length

$$l_b \equiv -\frac{a}{\ln \langle \cos \beta \rangle}. \quad (39)$$

Plugging in Eq. (36) and taking the limit $a \rightarrow 0$ yields

$$l_b = A \frac{1 - \frac{\varepsilon^2}{A^2} - \frac{G^2}{AC} \left(1 + \frac{\varepsilon}{A} \right)}{1 - \frac{G^2}{2AC}}. \quad (40)$$

In a similar manner (see for example [3]) one can define a correlation length associated with twist as follows

$$l_t \equiv -\frac{a}{2 \ln \langle \cos(\alpha + \gamma - 2\phi_0) \rangle}, \quad (41)$$

which, in combination with Eq. (37), gives

$$l_t = C \frac{1 - \frac{\varepsilon}{A} - \frac{G^2}{AC}}{1 - \frac{\varepsilon}{A}}. \quad (42)$$

Notice that for the standard TWLC model, i.e. for $\varepsilon = G = 0$, these correlation lengths reduce to $l_b = A$ and $l_t = C$. In the MS model, however, the twist-bend coupling and the bending anisotropy will make the rod more flexible, as $l_b < A$ and $l_t < C$.

Finally, let us neglect the twist-bend coupling $G = 0$ and focus on the effect of the asymmetric bending. In this case Eq. (40) yields

$$\frac{1}{l_b} = \frac{A}{A^2 - \varepsilon^2} = \frac{1}{2} \left(\frac{1}{A_1} + \frac{1}{A_2} \right), \quad (43)$$

i.e. the bending persistence length is the harmonic mean of the two bending constants. This is a known result [4,5] for the worm-like chain with bending anisotropy. Moreover, it follows from Eq. (42) that if $G = 0$ the twist persistence length will simply be $l_t = C$, i.e. the same as for the standard TWLC model.

Comparison with simulations

Equations (40) and (42) are exact in the continuum limit $a \rightarrow 0$. Here we compare them with simulation data, as a means of testing the computer model we employed for the numerical calculations. The simulations are based on a bead-and-spring model, in which each bead carries three patches. The latter introduce an intrinsic reference frame, which is used for the calculation of the relative bend and twist between consecutive beads. Our model is a greatly modified version of the one discussed in [3], with the addition of twist-bend coupling and bending anisotropy. For the simulations we are using the LAMMPS molecular dynamics simulation package [18][6].

As a first test, we studied the effect of the bending anisotropy and the twist-bend coupling separately. More specifically, we ran simulations for $G = 0$ and measured the dependence of the bending l_b and twisting l_t persistence lengths on ε . The results are summarized in Figs. 5a and 5b, where we also compare with the expressions

$$\frac{l_b}{A} = 1 - \frac{\varepsilon^2}{A^2} \quad \text{and} \quad \frac{l_t}{C} = 1, \quad (44)$$

as predicted by Eqs. (40) and (42). In a similar manner, we set $\varepsilon = 0$ and varied G , so as to compare with the theoretical predictions

$$\frac{l_b}{A} = \frac{1 - \frac{G^2}{AC}}{1 - \frac{G^2}{2AC}} \quad \text{and} \quad \frac{l_t}{C} = 1 - \frac{G^2}{AC}. \quad (45)$$

The output of the simulations, together with these expressions, are plotted in Figs. 5c and 5d. In all cases we observe a good agreement between the two.

Furthermore, we tested the combined effect of the bending anisotropy and the twist-bend coupling, by keeping one of the two properties fixed, while varying the magnitude of the other. More specifically, in Figs. 6a and 6b we show how l_b and l_t depend on ε , when setting $G = 20$ nm. Similarly, in Figs. 6c and 6d we have taken $\varepsilon = 20$ nm and plotted the G -dependence of the persistence lengths. Again, the agreement between theory and simulations is very good, even under this extreme ‘‘softening’’ of the rod.

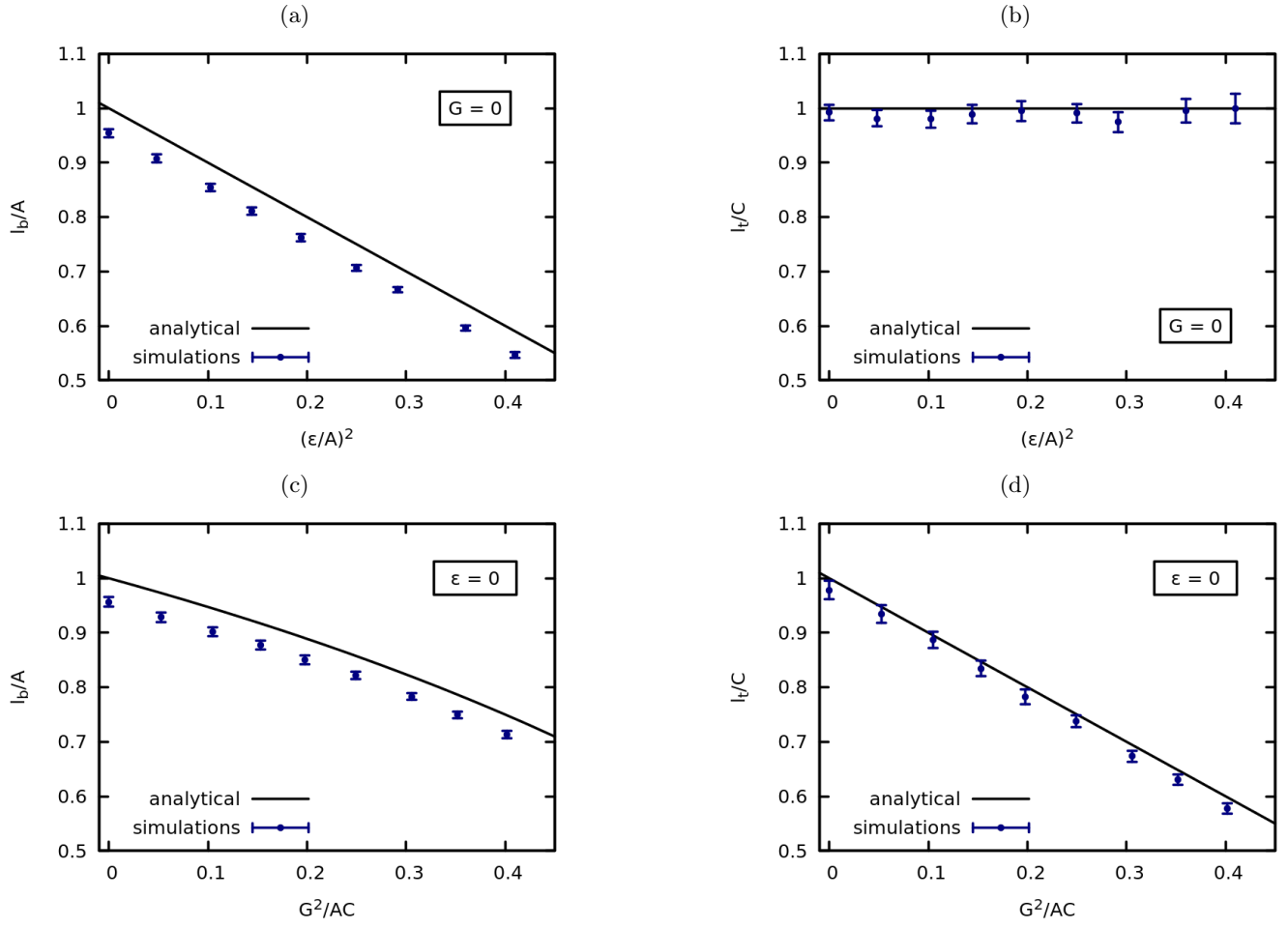


FIG. 5. Comparison between Eqs. (40) and (42) (solid lines) and computer simulations (points), showing how the bending l_b and twisting l_t persistence lengths are affected when one introduces the anisotropic bending ((a) and (b)) and the twist-bend coupling ((c) and (d)) separately. In both cases theory and simulations are in good agreement.

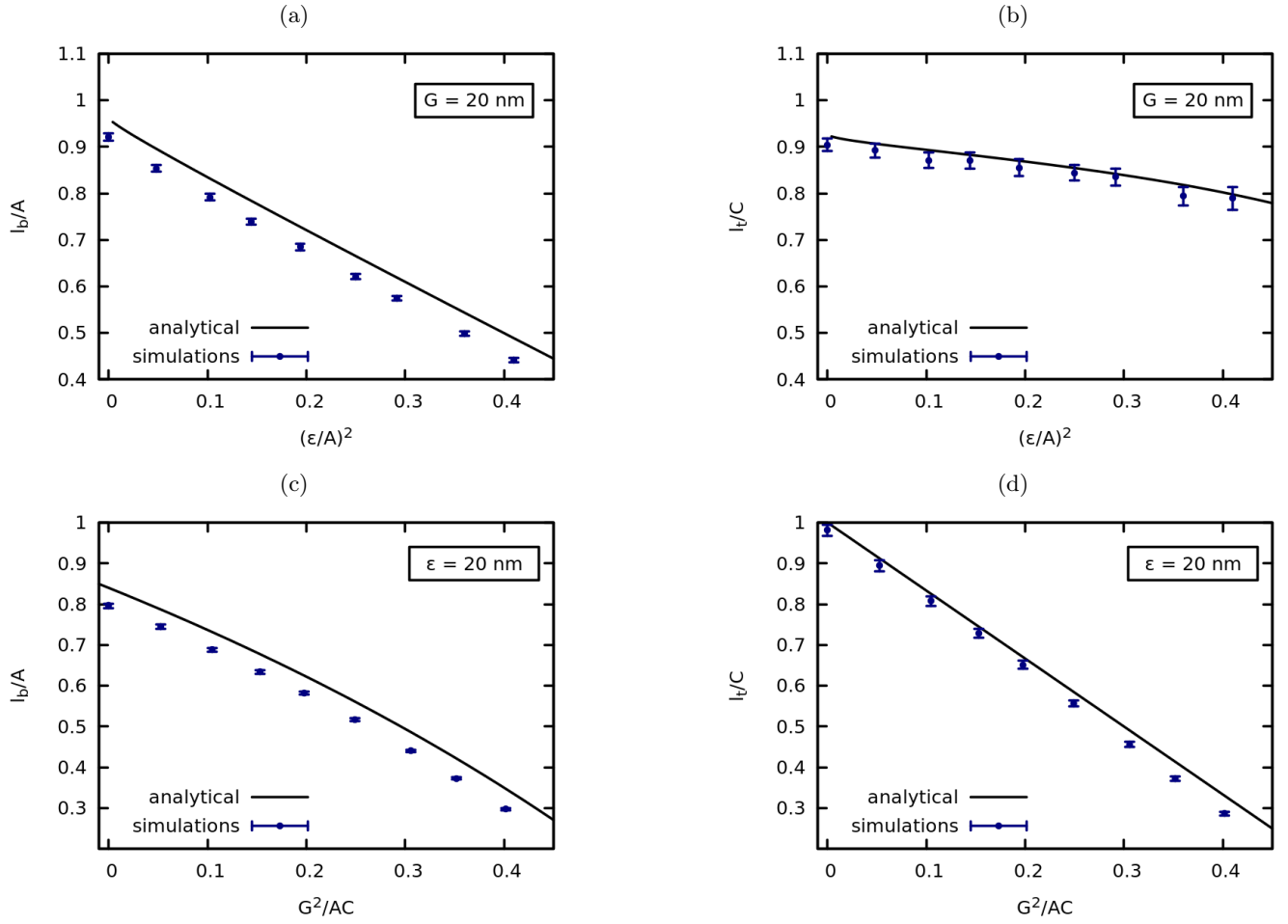


FIG. 6. Comparison between Eqs. (40) and (42) (solid lines) and computer simulations (points), showing how the bending l_b and twisting l_t persistence lengths are affected when one introduces both the anisotropic bending and the twist-bend coupling simultaneously. In (a) and (b) we display the dependence of l_b and l_t , respectively, on the bending anisotropy ϵ , with the twist-bend coupling constant being fixed at $G = 20$ nm. In a similar manner, in (c) and (d) we fix the bending anisotropy constant $\epsilon = 20$ nm and vary G . In all cases, the agreement between theory and simulations is very good.

[1] A quadratic form in the variable Ω_i is a homogeneous polynomial of degree two in those variables. It can be written in general by means of a symmetric matrix M_{ij} as $\sum_{ij} \Omega_i M_{ij} \Omega_j$. The quadratic form is said to be positive if the matrix M has positive eigenvalues. We require positivity in order for the system to be stable. In this case $\Omega_i = 0$ corresponds to the minimum value of the form.

[2] In the above calculation we have not dealt with the integration domain of χ very carefully. In the original partition function α and γ vary in the domain $-\pi \leq \alpha \leq \pi$ and $-\pi \leq \gamma \leq \pi$. When changing variables to ψ and χ the integration domain becomes a square with the sides tilted of 45° with respect to the ψ and χ axes. In Eq. (35) we integrate on $-\infty < \psi < \infty$ and $-\pi \leq \chi \leq \pi$. The extension of the integration of ψ to the whole real domain is justified by the Gaussian approximation. This is a good approximation except at the two “edges” of the original integration domain $\psi = 0$, $\chi = \pm\pi$. It can be shown that the correct calculation produces higher order terms in the discretization length a , compared to the result of (35).

[3] C. Brackley, A. Morozov, and D. Marenduzzo, *J. Chem. Phys.* **140**, 135103 (2014).

[4] F. Lankas, J. Sponer, P. Hobza, and J. Langowski, *J. Mol. Biol.* **299**, 695 (2000).

[5] B. Eslami-Mossallam and M. Ejtehadi, *J. Chem. Phys.* **128**, 125106 (2008).
